# Can Artificial Potentials Suit for Collision Avoidance in Factory Floor?
## *A Case Study of Harmonic Machine-machine Coexistence*

Josias G. Batista[1], José L. N. da Silva[1] and George A. P. Thé[2]
[1]*Instituto Federal de Educação Tecnológica do Ceará, av. 13 de Maio 2081, Fortaleza, Brazil*
[2]*Department of Teleinformatics Engineering, Federal University of Ceara, Fortaleza, Brazil*

Keywords: Path Planning, Machine-machine Interaction, SCARA Manipulator.

Abstract: Despite the existence of well-known approaches for collision prevention in the robotics literature, in present days the use of manipulators in fabrication processes still relies on safe-zone delimitations, which ultimately limits automation flexibility. In the present work, we consider going over that paradigm by discussing what if mobile agents of the fabrication process, i.e., robots could share the same space. In doing that study, the very classical approach based on artificial potentials for collision prevention are preferred over modern choices. On the basis of a hypothetical pick-&-place task experiment, results revealed efficient accomplishment in some of the considered scenarios.

## 1 INTRODUCTION

In modern production processes the deployment of robots in semi- or fully-automatized taks assumed an important and strategic role for industry; recent reports from the International Federation of Robotics estimate something over 250 thousands new units of industrial robots worldwide only in 2015 (IFR, 2017). Typically, industrial robots operate inside proper cells in classified areas designed to provide adequate separation between men and machines; it is also recommended the use of sensors for human-presence detection as well as switching-off mechanism in case of cell invasion by persons. It is to be stressed the economical consequence of it, since interrupting the process may cause delays and bring additional production costs.

From the point-of-view of increasing flexibility level of automation, it would be good thing if those strict recommendations for robot cells could be revisited and production machines and other agents were let free to share the factory floor aided by techniques for preventing collisions and process interruptions as well. This issue may be regarded as a machine-machine coexistence problem and it is a challenging one if no previous information about dimension and shape of the agents is given as well as the agents are allowed to move arbitrarily in that space, as illustrated in Figure 1. To cover with the need for a non-stop production, an intelligent robot-assisted automation system should therefore conjugate real-time obstacle detection and collision avoidance algorithms.

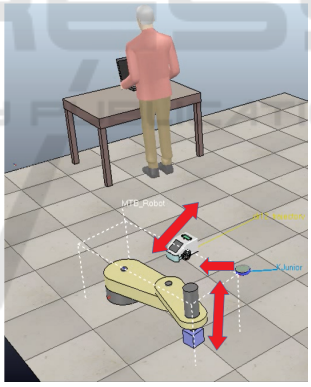

Figure 1: Various robots sharing workspace.

In the literature, the paradigm of machine-machine interaction is usually presented as cooperative robotics, in which agents has a common task to accomplish (Habib, 2014) or, in the context of assistive robotics, in which robots interact to anticipate human actions thus offering them some kind of assistance like, for instance, in helping at opening a door, taking up objects, etc (Koppula and Saxena, 2016). Also interesting is the context of competitive robotics, in which machines interact as opponents (Pinto et al., 2016) or more simply in situations of conflicting interests (e.g., those of workspace superposition) (Gayle et al., 2007).



Batista, J., Silva, J. and Thé, G.
Can Artificial Potentials Suit for Collision Avoidance in Factory Floor? - A Case Study of Harmonic Machine-machine Coexistence.
DOI: 10.5220/0006832405470556
In *Proceedings of the 15th International Conference on Informatics in Control, Automation and Robotics (ICINCO 2018) - Volume 2*, pages 547-556
ISBN: 978-989-758-321-6

Right in this context the present research is focused: it brings to light a hypothetical automatized production process in which mobile robots and manipulators are the agents having conflicting tasks by discussing how the machine-machine interaction can be driven towards more efficient and productive process (Moellmann et al., 2006). The scenario considered here is the one illustrated in Figure 1: two automatic machines with overlapping workspaces share a given region of the factory floor and have to deal with the possibility of iminent collision; the manipulator is doing a pick-and-place task, whereas the wheel-drive robot is on some transport task in non-constrained route. The more collisions occur, clearly the more the robots will limit the efficiency of the productive process they are engaged in, because the timing and productivity metrics for performance evaluation will suffer from non-scheduled stops. Collisions are therefore to be avoided undoubtedly; nothing new. What is not known in advance and appears as open issue in this hypothetical experiment is the amount of influence the chosen strategy for collision avoidance may have on the on-going production. First of all, are the classical approaches for collision avoidance of robots viable for real-time navigation in the considered emulated production scenario? If so, under which assumptions and operating (or even modelling) constraints? Then, how can we quantify the influence the chosen collision prevention strategy has on the task assigned to the robot? Is there any measure from the scientific community to be used as indicator of the just mentioned quantity? Any opportunity for new measure or even a figure-of-merit?

Purpose of this paper is to address these questions through the use of classical approaches in robotics and traditional concepts from production engineering. On one side, concerning the strategy for collision prevention, in this study artificial potential fields was preferred over geometric search approach for its simplificity and popularity as the literature review reveals. On the other side, to evaluate task accomplishment, it was adopted an indicator named *Overall Equipment Efficiency*, which takes into account availability, quality and performance itself of a given machine.

The remainder of the paper is organized in the following sections: after a literature review about the employment of artificial potential field methods for path planning in robotics, section 3 presents the theoretical ingredients such as the manipulator kinematics, the adopted Fuzzy controller design, the basics of artificial potentials, as well as the metrics used to assess the efficiency of the transport task studied here. Section 4 contains the results and respective discussion, which are followed by conclusions.

## 2 LITERATURE REVIEW

Artificial potential field (APF) methods are very classical choice for reactive path planning of robots dealing with moving obstacles; originally proposed in (Khatib, 1986) for collision avoidance of manipulators and mobile robots as well, it is still very popular because it is fast, simple and mathematically elegant (Mora and Tornero, 2008), though it suffers from important limitations, such as the existence of local minima.

Despite its original use for path planning of manipulators, many sub-areas of the robotics community benefited from APF methods so far. In the work of (Mac et al., 2016), for example, APF was chosen to address path planning of unmanned aerial vehicles (UAV) under obstacle avoidance constraint, and in (Budiyanto et al., 2015) APF for UAV flight was preferred over laser scanning, computer vision and global positioning system based approaches. Underwater robotics was addressed by (Cheng et al., 2015); a new best-route strategy for unmanned robot navigation was designed from a velocity synthesis algorithm relying on APF based collision prevention. Authors in (Wang et al., 2015), in turn, combined APF and grid map method to design free-collision routes for mobile robot as a way to prevent trapping at local minima, whereas (Chatraei and Javidian, 2015) used APF for generating the path used as input of the Fuzzy-Mandani position and orientation controller of a mobile robot. Still in the sub-field of mobile vehicles, the interesting work of (Galceran et al., 2015) brought a car equipped with APF based trajectory generator able to deviate from static and moving obstacles in a real road. Concerning manipulators, APF was successfully used for static obstacle collision avoidance in (Hargas et al., 2015), for preventing contact with moving obstacles in (Guan et al., 2015; Ataka et al., 2016; Badawy, 2014) and also for surgery assistance in dental implants (Yu et al., 2015b; Yu et al., 2015a).

It is interesting that the above presented review of recent research did not consider any issues regarding a typical industrial environment in the studies, though we know it is the main destination of most manipulators deployed nowadays; this lack of discussion is one of the motivations for the present study.

# 3 THEORETICAL BACKGROUND

## 3.1 Overall System View

The overall system view is shown in the diagram illustrated in Figure 2. Starting from top-view image acquisition by a PMD 3D Effector camera from ifm electronic gmbh ©and some digital image processing techniques in a computer, the obstacle is identified in a given scene and represented as circle object. Then, the region it occupies in cartesian space is mapped to generate the prohibited configuration space, thus allowing the use of APF to find a free-collision path to the goal point. A smooth trajectory is then calculated and sent via OPC communication link to the Fuzzy controller embedded in the PLC for driving the motors accordingly. This is repeated until goal point is reached by the manipulator end-effector.

The industrial robot used in this experiment is a retrofitted 4-DOF SCARA, from Toshiba ©, whereas the robot playing the role of moving obstacle is a Zumo Robot from Pololu Robotics and Electronics ©. The PLC is a TwidoSuite from Schneider Electric ©.

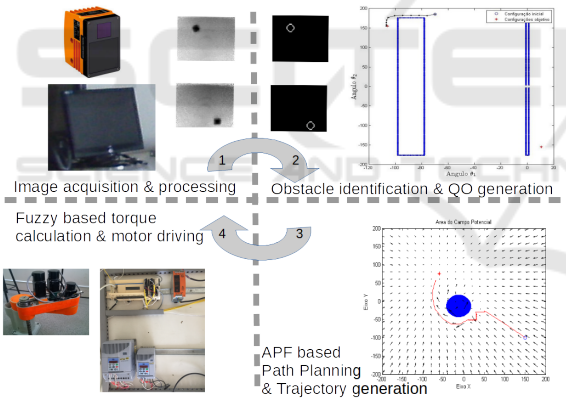


Figure 2: Overall view of the closed-loop system.

## 3.2 Manipulator Kinematics

In the experiments to be discussed next, only planar movements were investigated. This was due to lack of enough driving units for the whole set of 4 joint motors, what limited the path planning to 2D space only. However, for completeness, in the following the full-set of Denavit-Hartenberg (DH) parameters for direct kinematics, as well as the equations for inverse kinematics are reported.

Figure 3 shows the various robot parameters and frame assignment according to DH convention. As seen in the illustration, joints 1, 2 and 4 are rotational, whereas joint 3 is a prismatic one. Table 1 brings

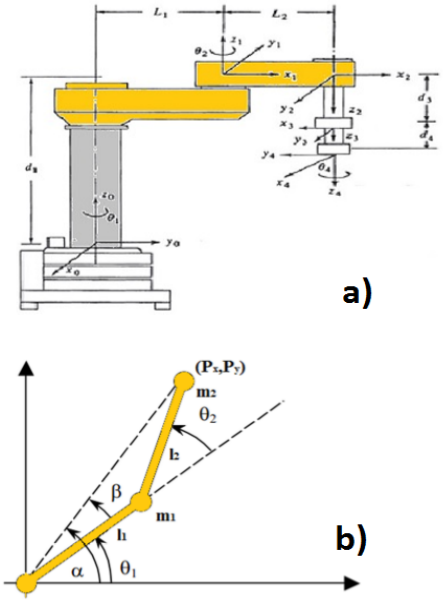


Figure 3: Illustration of the SCARA manipulator: a) with assigned references frames; b) in-plane projection of principal revolute joints.

the values of the whole set of parameters needed for deriving kinematic equations.

Table 1: DH parameters of the manipulator.

| Axis | $\theta_i$ | $d_i$ | $a_i$ | $\alpha_i$ |
|---|---|---|---|---|
| 1 | $\theta_1$ | $d_1 = 0.32$ | $L_1 = 0.35$ | 0 |
| 2 | $\theta_2$ | 0 | $L_2 = 0.30$ | $\pi$ |
| 3 | 0 | $d_3$ | 0 | 0 |
| 4 | $\theta_4$ | $d_4$ | 0 | 0 |

The adopted convention and the above parameters allow for obtaining the homogeneous transformation matrix relating initial and final frames as:

$$T = \begin{bmatrix} S_4S_{12}+C_4C_{12} & S_4C_{12}+C_4S_{12} & 0 & T_{14} \\ S_4C_{12}+C_4S_{12} & -S_4S_{12}+C_4C_{12} & 0 & T_{24} \\ 0 & 0 & -1 & T_{34} \\ 0 & 0 & 0 & 1 \end{bmatrix}, \quad (1)$$

where : $S_{12} = sen(\theta_1+\theta_2)$ , $C_{12} = cos(\theta_1+\theta_2)$, $T_{14} = l_1C_1+l_2C_{12}$, $T_{24} = l_1S_1+l_2S_{12}$ and $T_{34} = d_1-d_3-d_4$.

## 3.3 SISO Closed-loop Fuzzy Control

Manipulators driven by electric motors usually counts on reduction gears based transmission system to improve torque and for reducing speed. If on one side it raises costs, the amount of parts and the rotating inertia, on the other side it may lead to improved positioning since the links can undergo displacements of

small magnitude. As discussed in (Spong, 2006), manipulators having that driving characteristic may be treated as a SISO system since the gear ratio, β be among 20 and 100, in such a way that load inertial effects may be neglected, thus allowing for independent control (Mittal and Nagrath, 2003). For the manipulator of the present work, whose actuating units are based on permanent magnet electric motors with no slip, an experiment was performed to estimate the gear ratios at the joints, $\beta_1$ and $\beta_2$. By setting the frequency inverter to3 Hz, the time required for the joint to complete a 90º rotation was recorded and the number of revolutions of the motor axis was estimated (see, for instance, (Fitzgerald et al., 2014)), thus yielding the ratios presented in Table 2. In the table, the symbol # stands for "the number of revolutions of".

Table 2: Data collected from gear ratio estimation.

| Joint | *Time* | *#Motor* | *#Joint* | β |
|---|---|---|---|---|
| 1 | 13.35 | 20.025 | 0.25 | $\beta_1 = 80.1$ |
| 2 | 8.60 | 12.897 | 0.25 | $\beta_2 = 51.6$ |

The above calculated gear ratios justify the adoption of joint independent control, and then a SISO zero-order Takagi-Sugeno Fuzzy controller was designed for each joint (Farooq et al., 2011). The only reason for adopting this strategy instead of classical PID or even hybrid PID-Fuzzy is that in our preliminary studies, the proposed Fuzzy-TS showed to be superior in accuracy and repeatability measurements done according to (ISO, 1998). For what concerns the controller design itself, most of it relied on theoretical concepts as well as authors' experience in manipulator control and agreed with the independent work of (Nawrocka et al., 2014). As input variables, the joint position error was calculated from the difference between desired and measured angular position; it was limited to the interval [-30;30] in units of internal CLP memory, what means [-2.63º; 2.63º]. Those values are in accordance with the positioning-task purpose of this experiment. The error fuzzy variable following the defuzzying step is defined from five membership functions, chosen among trapezoidal- and triangular-like choices as represented in:

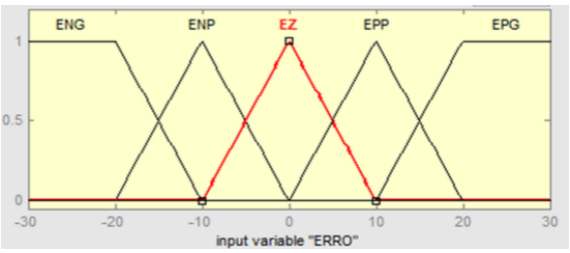


Figure 4: Adopted membership functions for input variable error.

The choice for these simples functions is due to the limited programming resources in the PLC available to host the Fuzzy controller. In addition, the symmetry around the origin as well as the 50% overlap among adjacent functions makes simpler the ladder enconding of the proposed controller, since the denominators at the defuzzying step get to unity while favouring the triangle functions to be replaced by linear parts (Simoes and Shaw, 2007).

Concerning the output variable generated by the Fuzzy controller, the following constants are defined: K1=-10, K2=-5, K3=0, K4=5 e K5=10; they respectively encode the fuzzy variables TNG, TNP, TZ, TPP, TPG. The interval [-10;10] for the output is associated to the 0-10V analog range of the PLC output used to for motor driving, with positive or negative values yielding clockwise or anticlockwise rotation direction, respectively. The adopted interval also prevents actuator saturation. Finally, five very simple fuzzy rules were adopted for the position control task:

If EPG then TNG; If EPP then TNP; If EZ then TZ; If ENP then TPP; If ENG then TPG;

### 3.4 Integration of APF to the Control System

In a few words, artificial potential field method for free-collision robot motion relies on the existence of artificial repulsive potential fields caused by obstacles, $U_{rep}(q)$, and artificial attractive potential field centered at the target (final) position, $U_{att}(q)$, guiding the robot according to the experienced virtual force:

$$\mathbf{F}(\mathbf{q}) = -\nabla U(\mathbf{q}), \tag{2}$$

where

$$U(\mathbf{q}) = U_{rep}(\mathbf{q}) + U_{att}(\mathbf{q}). \tag{3}$$

Usual choices for these potential consider functions having first derivative continuous and smoothly changing. In the experiments reported here, the attractive potential was built by combining the conical and parabolic functions (Volpe and Khosla, 1990):

$$U_{atr}(\theta) = dK_a \parallel \theta - \theta_f \parallel - \frac{1}{2}d^2K_a \; : \parallel \theta - \theta_f \parallel > d, \tag{4}$$

$$U_{atr}(\theta) = \frac{1}{2}K_a \parallel \theta - \theta_f \parallel^2 : \parallel \theta - \theta_f \parallel \leq d, \tag{5}$$

where $K_a$ is a constant, θ is the joint position at a given time instant and $\theta_f$ is the desired joint position at the goal point; $d$ defines the transition limit between conical and parabolic actions. The parameters are set $K_a = 1$ and $d = 2cm$ in the experiments reported here.

The repulsive potential, in turn, resembles the following flat-sided function:

$$U_{rep}(\theta) = \frac{1}{2}K_r[\frac{1}{p(\theta)} - \frac{1}{p}]^2 \ : \ p(\theta) \leq p, \quad (6)$$

$$U_{rep}(\theta) = 0 \ : \ p(\theta) > p, \quad (7)$$

in the above equations, $K_r$ is a constant, $p(\theta)$ represents the minimal distance between the joint position , $\theta$, and the whole configuration space of a given obstacle, $QO$. At last, $p$ defines a limit line in configuration space where the robot can not feel the presence of that obstacle.The parameters are set $K_r = 5000$ and $p = 2cm$ in the experiments reported here.

The present implementation of the APF in the present work counted on the use of an image sensor for continuous capture of the scene; this allowed, in turn, for the calculation of the QO-space in continuous operation and the generation of free-collision paths. To calculate the QO-space, an image processing algorithm was developed for detection and localization of the wheeled robot; robot speed was limited to mitigate the effects of the delay between wheeled robot detection and the manipulator decision on movement update. Clearly, the events define the time window in which the artificial potential field estimates a free-route.

As it will become clearer in section 3.5, this implementation of APF considered different levels of description for the manipulator and for the wheeled robot, namely as a point or an extended body. For what concerns the manipulator, considering it as a point has the consequence of applying APF equations for repulsive field between the end-effector only and the obstacle, whereas when taken as a body, the repulsive potential accounts for the interaction between the obstacle and many different points throughout the arm (known as control points).

Things are similar for wheeled robot: when taken as a point, the repulsive potential is calculated according to its distance to the manipulator end-effector (if this is taken as a point) or to the various control points. On the other side, if the wheeled robot is regarded as a body, a line circle centered at its centroid coordinates plays the role of obstacle and, hence, spatial sampling along this line defines several control points, as well. This ultimately augments the obstacle space, since each of the control points now work as a different obstacle.

From this discussion, it should be clear that the APF computation is highly demanding in the body-body scenario mentioned latter in this paper.

## 3.5 Investigated Scenarios

Eight scenarios were designed to study the hypothetical transport experiment reported in this paper. To compose this set of scenarios two main reasoning lines were followed; one of them regards the geometry, i.e., the dimensions of both robots, whereas the other is about the accomplishment of the task itself.

The APF was originally conceived for automatic motioning in which the mobile robot is generally taken as a point. Same story for the manipulator; usually the end-effector is the only portion of the robot subject to the potential fields. But what if they are treated as extended bodies, i.e., their actual dimensions are not neglected? Roboticists know that the complexity of APF algorithm grows with the definition of control point along the manipulator open-chain and with the number of contact points in the surface of an obstacle (or, similarly, with the amount of them).

The other issue regards the accomplishment level of the transport mission: is position uncertainty acceptable in placing task? Although precision robotics is a very attractive field in its own, many industrial processes do not impose strict constraints for position or orientation of objects; therefore, reaching a zone instead of a specific location may suffice sometimes.

Those arguments were essential to propose the methodology adopted so far; on one hand, it consists of describing the robots as a point (P, for short) or as an extended body (B, for short), thus giving 4 combinations for the couple *(manipulator robot, wheeled robot): (P,P); (P,B); (B,P); (B,B)*. On the other hand, for what concerns the task itself, two missions were considered according to the degree of task accomplishment: mission-T (target) and mission-Z (zone). By mission-T it is meant the manipulator task which requires the object be placed at a specific point at the goal, whereas the mission-Z is less restrictive in the sense that the object may be left in the vicinity of the goal position (10 cm around the goal was adopted in the experiments).

## 3.6 Measuring Task Efficiency

To assess the efficiency of the manipulator in repeatedly doing the hypothetical pick-place task illustrated in Figure 1, the eight scenarios just described were investigated. On doing that, two measures have been considered to quantify the efficiency of the repetitive pick-place, which will be described in the following.

### 3.6.1 Proposed Efficiency

In order to quantitatively assess the efficiency of the robotic system in the pick-&-place task, we proposed

a simple equation taking into account the productivity itself, the variability of time elapsed in each repetition of the task and the amount of collision events as well. This function is a figure-of-merit and works somehow as an indicator of the influence of the APF method on the considered hypothetical process, and that is why it is named efficiency, $\eta$. The proposed efficiency is proportional to what we call productivity and inversely proportional to the variance of the elapsed time and to the number of collisions, according to:

$$\eta = \frac{P_{rod}}{\sigma_{temp} N_{col.}}, \tag{8}$$

where $P_{rod}$ is the productivity, which means the number of times the mission was successfully complete, i.e., the transport from origin to goal did not suffer any collision, $\sigma_{time}$ is the variance of the time spent in every repetition of the transport and $N_{col}$ is the amount of collisions recorded.

#### 3.6.2 Overall Equipment Effectiveness

Although its simplicity, the proposed formula for task effiiciency is not usual in industry. More adequate is the use of measurements derived from the total productive maintenance (TPM), originally developed in Japan for preventing wastes and reducing non-programmed stops, thus ensuring quality and cost save in continuous processes. One example is the Overall Equipment Effectiveness (OEE) (Kennedy, 2017), which is a measure of manufacture systems for equipment evaluation relying on its performance, availability and quality. In the following it is discussed how to interpret the hypothetical pick-&-place problem in order to measure the robotic system efficiency using this OEE concept.

Availability: its a percentage of the time spent in effective working condition compared to the total time available for operation, and is calculated as it follows:

$$A_{vail}(\%) = \frac{TTD - PP - PNP}{TTD - PP} * 100, \tag{9}$$

where TDD is the total time available for operation, PP is the time reserved for programmed stops and PNP is the time spent in non-programmed stops. In the experiments reported in this work, we considered no programmed stops at all; in addition, we associate the non-programmed stops to the interruptions due to collision prevention actions of the manipulator or to some set-up adjustment. Then, to calculate the availability, TDD and PNP were both recorded.

Performance: it consists in a relation between the quantity of parts really produced by the machine and the expected amount, when considering the cycle time. In other words, it measures the production rate of a given equipment, and is calculated as it follows:

$$P_{erf}(\%) = \frac{TEO}{TO} * 100, \tag{10}$$

where TEO is the operating effective time and TO is the operating time. To calculate the performance in the present work, we considered TO as the time in which the manipulator was in movement, since the operation here is regarded as transport rather than fabrication itself; the other parameter, TEO, was computed also as a time-in-movement parameter, but provided exclusion of unsuccessful mission repetitions (e.g., with collision events).

Quality: it refers to the existence of defective products ultimately resulting in rejection or rework. Since in the experiments we have done so far there is no fabrication at all, we considered the quality, $Q_{uali}$ at 100% in equation 11 below.

OEE indicator: it is expressed as the product of the three metrics just defined according to

$$OEE(\%) = A_{vail} * P_{erf} * Q_{uali} * 100 \tag{11}$$

### 3.7 Required Energy Estimation

Also the torque and required energy were estimated in the various tests performed. A look at the energy consumption is important because it may influence the decisions at the factory level. As any problem in engineering, it is pursued a good trend between the benefits of new approaches for manufacturing and the additional costs brought. This could help answering the following questions: a) can the factory afford the adoption of an automatic collision avoidance system? Is the raising of energy costs acceptable? Is the productivity increase worth the rise of energy consumption?

In doing this analysis, it has been seen that joint 1 showed superior power demand respect to joint 2. For this reason, in the tables reporting those quantities, only joint 1 numbers will be presented. Torque and energy calculations followed the approach of (Fitzgerald et al., 2014) and will be summarized in the following.

Initially, we take an estimation of the torque at joint motor 1, $T_{m1}$ from:

$$T_{m1} = 9.55 \frac{P_{m1}}{N_{m1}}, \tag{12}$$

where $P_{m1}$ is the nominal power in $W$ coming from plate specifications and $N_{m1}$ is the rotating speed in $min^{-1}$. The values for rotating speed were obtained from the PLC output sent to the frequency inverter

driver. Since this is a permanent magnet synchrounous motor, it shows no slip and, as such, its rotating speed can be determined from:

$$N_{m1} = \frac{120f}{P}, \tag{13}$$

where $f$ is the frequency inverter driver output and is measured in $Hz$, whereas $P$ is the number of poles.

Solving equation 12 for the developed power and using the derivative of angular position at joints as a measure for the rotating speed, one can use the following equation to estimate the power in $kW$:

$$P_{m1} = \frac{T_{m1}V_{m1}}{9549.2965}, \tag{14}$$

where $T_{m1}$ comes from equation 12 and $V_{m1}$ is the estimation for the joint 1 rotating speed from enconders. The required energy, $E$, can then be estimated by integrating the developed power over time, $P_{m1}$:

$$E = \sum_{i=1}^{n}(P_{m1i}t_i). \tag{15}$$

# 4 RESULTS AND DISCUSSION

For every scenario described in section 3.6, they were recorded the number of mission repetitions and respective elapsed time, amount of collision events, number of interruptions due to collision prevention and the number of accomplished missions (productivity). Those quantities were then used to calculate the task efficiency according to the formulae presented earlier are reported in Table 3. It is worth mentioning that also the time spent during the interruptions for preventing collisions were recorded.

A look at the table reveals that the scenario (P;B) led to better productivity and less collisions for both missions considered. Also interesting to note that no manipulator stop was observed. The scenario (B;B) instead led to low productivity, though only one collision event has occurred; interestingly, there were events of manipulator stops to avoid collision, though the mission was not accomplished in those rounds. This may be connected to the artificial potential field method: since the manipulator is here a extended-body, the obstacle configuration space gets larger, and hence the algorithm can not find a free-space towards push the manipulator to end the mission. For what concerns the efficiency of task accomplishment, results reveal that in the scenarios considering the manipulator as extended-body the efficiency falls; we associate this to the same lack of free-space just discussed.

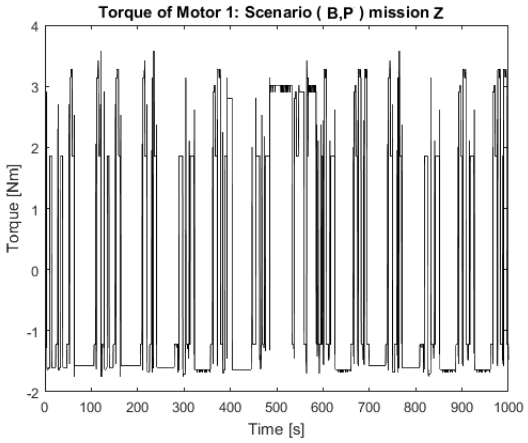


Figure 5: Time-series for motor 1 torque [Nm] in scenario *(B,P)*, mission-Z.

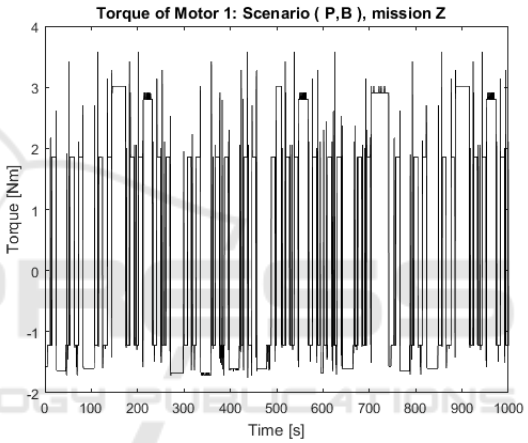


Figure 6: Time-series for motor 1 torque [Nm] in scenario *(P,B)*, mission-Z.

In the scenario (P;P) the manipulator is again regarded as a point, but, this time, collision events raise. This is because in this scenario also the obstacle is considered as a point, what means that the repulsive field pushing the manipulator away is weaken. This ultimately led to low task efficiency.

Using now the OEE indicator as efficiency measure, we could see that results agreed. The scenario (P;B) reached 67.47% and 67.82% for missions-T and -Z, respectively. We believe the tiny advantage of mission-Z is because it imposes less constraints to the artificial potential field method, speeding up the process as whole. According to (Kennedy, 2017), those numbers fall withing the interval [65% - 75%] for the OEE, making them acceptable, though the universal recommendations point to 85% as a goal.

Switching the attention to the required energy, results in the table show more demand in the scenario (P;B) for both missions. We associate this to the motor excitation along time, as reported in Figures 5 and

Table 3: Summary of experimental results in the different scenarios evaluated.

| **Scenario** | **Mission-T** | | | | | | | | | | |
|---|---|---|---|---|---|---|---|---|---|---|---|
| | Trials | Time $[s]$ | Bumps | $P_{rod}$ | Stops | $\eta$ | $\sigma_t$ | $A_{vail}$ | $P_{erf}$ | OEE $[\%]$ | Energy $[kWh]$ |
| (B,B) | 27 | 182.42 | 3 | 20 | 4 | 1.333 | 4.989 | 59.08 | 74.92 | 44.27 | 0.0041 |
| (B,P) | 29 | 171.04 | 6 | 18 | 5 | 0.704 | 4.258 | 60.00 | 70.84 | 42.71 | 0.0032 |
| (P,B) | 36 | 230.36 | 5 | 31 | 0 | 8.324 | 0.744 | 76.99 | 87.64 | 67.47 | 0.0058 |
| (P,P) | 35 | 198.17 | 6 | 29 | 0 | 3.491 | 1.384 | 42.17 | 88.37 | 37.27 | 0.0042 |
| **Scenario** | **Mission-Z** | | | | | | | | | | |
| (B,B) | 32 | 207.96 | 1 | 27 | 4 | 6.921 | 3.901 | 40.62 | 88.95 | 36.13 | 0.0037 |
| (B,P) | 29 | 146.70 | 3 | 23 | 3 | 5.614 | 1.365 | 56.62 | 84.16 | 47.65 | 0.0021 |
| (P,B) | 35 | 213.22 | 3 | 32 | 0 | 12.465 | 0.855 | 73.36 | 92.44 | 67.82 | 0.0051 |
| (P,P) | 35 | 210.92 | 7 | 28 | 0 | 3.303 | 1.210 | 73.04 | 85.07 | 62.14 | 0.0040 |

Table 4: Statistics of the error between desired and real joint positions.

| **Scenario** | **Mission-T** | |
|---|---|---|
| | Mean (std dev) joint 1 | Mean (std dev) joint 2 |
| (B,B) | 3.100 ($\pm$ 1.017) | 2.979 ($\pm$ 0.995) |
| (B,P) | 0.975 ($\pm$ 1.677) | 3.280 ($\pm$ 1.159) |
| (P,B) | 1.086 ($\pm$ 1.360) | 4.568 ($\pm$ 1.899) |
| (P,P) | 1.458 ($\pm$ 0.985) | 4.090 ($\pm$ 2.593) |
| **Scenario** | **Mission-Z** | |
| (B,B) | 3.177 ($\pm$ 1.027) | 3.503 ($\pm$ 1.052) |
| (B,P) | 0.692 ($\pm$ 1.200) | 3.009 ($\pm$ 1.158) |
| (P,B) | 1.167 ($\pm$ 1.209) | 4.037 ($\pm$ 2.408) |
| (P,P) | 1.592 ($\pm$ 1.396) | 4.382 ($\pm$ 2.470) |

6: more inversion peaks means clearly that the motor worked harder, thus leading to high productivity. We can therefore state that higher productivity and better efficiency led to high energy demand. The authors found this discussion relevant because it links the path planning problem, which is a robotic one, to the machine maintenance issue. Indeed, higher motor excitation implies higher acceleration and breaking levels during task operations. This analysis should ultimately influence the choice among the scenarios considered in the study.

Finally, we have studied the performance of this hypothetical pick-place system at low level, i.e., at the level of trajectory-following in configuration and in cartesian spaces. The goal here is to check how good was the designed controller in following the path calculated by the trajectory planner. In other words, we check here the difference (or error) between the desired and measured values of the joint angular position along time during the robot operation. Table 4 brings the average error and its standard deviation for every scenario considered so far.

For better comprehension, we emphasize that error measures were calculated over time within a given mission, and then over different mission repetitions. In other words, every time the manipulator started a transport mission from origin to goal position, the measured and desired joint position were used to create a time-vector of residuals. Then, average was calculated from it, and finally this number was recorded. Successive repetitions of the pick-&-place mission gave rise to a new error outcome. After several mission repetitions, the statitics presented in Table 4 were available.

To illustrate the performance of the designed Fuzzy controller when aided by the path-planner based on artificial potentials, we chose two antagonic scenarios concerning the productivity tooking care to consider different missions. In Figures 7 and 8 we plot, in cartesian space, the desired and real paths at different moments of the pick-&-place task. The scenarios considered in this part of the experiment were (B;P) mission-Z in Figure 7 as a low-productivity sample, and (P;B) mission-T in Figure 8 as a high-productivity sample. Unlike the analysis of productivity, here the scenario (B;P) showed superior performance, revealing that high productivity comes at the expense of innacurate trajectory-following.

## 5 CONCLUSIONS

In the present work a hypothetical production process with non-cooperative machine interaction was studied. Based on classical approaches, it consisted in providing a SCARA manipulator with the ability to prevent collisions in a workspace co-shared by a wheeled robot following random navigation, thus emulating what could be referred as conflicting tasks. Main goal of the study was to check the conditions for safe co-existence yet guaranteeing efficient task accomplishment. For that end, different scenarios were considered and different metrics for task efficiency

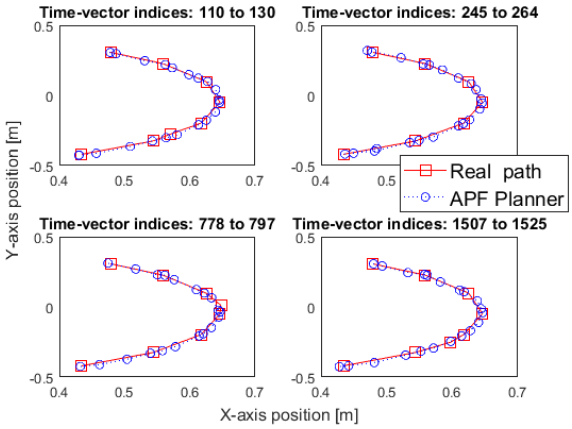


Figure 7: Cartesian space view of free-collision paths in scenario *(B,P)* mission-Z, in different repetitions of the pick-&-place operation. In each plot, blue line refers to the path generated by the APF planner, and red line refers to the path really followed by the robot.

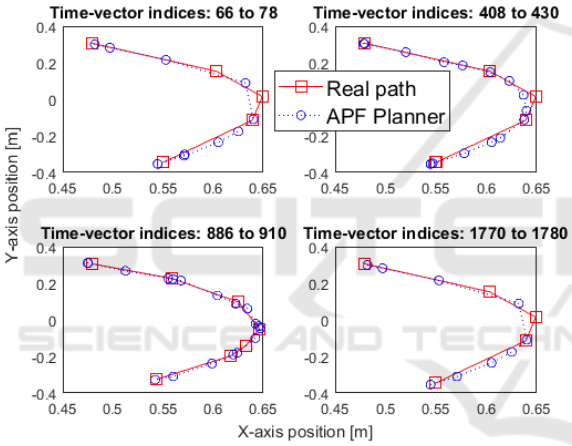


Figure 8: Cartesian space view of free-collision paths in scenario *(P,B)* mission-T, in different repetitions of the pick-&-place operation. In each plot, blue line refers to the path generated by the APF planner, and red line refers to the path really followed by the robot.

were analyzed. Although this work was not aimed at providing the scientific community with a general procedure for facing the safe co-existence of robots in industrial environments, we firmly believe that the considered case study may result useful for deployment of such techniques in factory-floor operations.

Among the various results discussed throughout the paper, it is worth to highlight that in a path planning strategy based on artificial potential fields, higher task efficiency is obtained when the manipulator is described as a point and the obstacle is considered as extended-body; this favours collision avoidance by keeping robot and obstacle away from each other while increasing the productivity due to better workspace usage. A second consequence of this scenario is that the low occurrence of collision events and non-programmed stops led to less fluctuation in mission times, thus implying in more productive robot operation.

According to metrics commonly used in process and fabrication management, the hypothetical process emulated in this study reached acceptable levels of effectiveness, since the estimated OEE amounts to about 68%. This study could motivate engineers and practitioners to consider new paradigms about the co-existence of moving machines in factory floor.

## ACKNOWLEDGEMENTS

Authors thank the Fundação Núcleo de Tecnologia Industrial do Ceará for administrative facilities.

## REFERENCES

Ataka, A., Qi, P., Liu, H., and Althoefer, K. (2016). Real-time planner for multi-segment continuum manipulator in dynamic environments. *2016 IEEE International Conference on Robotics and Automation (ICRA)*, pages 4080–4085.

Badawy, A. (2014). Manipulator trajectory planning using artificial potential field. In *Engineering and Technology (ICET), 2014 International Conference on*, pages 1–6. IEEE.

Budiyanto, A., Cahyadi, A., Adji, T. B., and Wahyunggoro, O. (2015). Uav obstacle avoidance using potential field under dynamic environment. In *Control, Electronics, Renewable Energy and Communications (ICCEREC), 2015 International Conference on*, pages 187–192. IEEE.

Chatraei, A. and Javidian, H. (2015). Formation control of mobile robots with obstacle avoidance using fuzzy artificial potential field. In *Electronics, Control, Measurement, Signals and their Application to Mechatronics (ECMSM), 2015 IEEE International Workshop of*, pages 1–6. IEEE.

Cheng, C., Zhu, D., Sun, B., Chu, Z., Nie, J., and Zhang, S. (2015). Path planning for autonomous underwater vehicle based on artificial potential field and velocity synthesis. In *Electrical and Computer Engineering (CCECE), 2015 IEEE 28th Canadian Conference on*, pages 717–721. IEEE.

Farooq, U., Hasan, K. M., Abbas, G., and Asad, M. U. (2011). Comparative analysis of zero order sugeno and mamdani fuzzy logic controllers for obstacle avoidance behavior in mobile robot navigation. In *Current Trends in Information Technology (CTIT), International Conference and Workshop on*, pages 113–119. IEEE.

Fitzgerald, A. E., Kingsley Jr, C., and Umans, S. D. (2014). *Electric Machinery*. McGraw-Hill, New York.

Galceran, E., Eustice, R. M., and Olson, E. (2015). Toward integrated motion planning and control using potential fields and torque-based steering actuation for autonomous driving. In *2015 IEEE Intelligent Vehicles Symposium (IV)*, pages 304–309. IEEE.

Gayle, R., Sud, A., Lin, M. C., and Manocha, D. (2007). Reactive deformation roadmaps: motion planning of multiple robots in dynamic environments. In *Intelligent Robots and Systems, 2007. IROS 2007. IEEE/RSJ International Conference on*, pages 3777–3783. IEEE.

Guan, W., Weng, Z., and Zhang, J. (2015). Obstacle avoidance path planning for manipulator based on variable-step artificial potential method. In *The 27th Chinese Control and Decision Conference (2015 CCDC)*, pages 4325–4329. IEEE.

Habib, M. K. (2014). *Handbook of Research on Advancements in Robotics and Mechatronics*. IGI Global.

Hargas, Y., Mokrane, A., Hentout, A., Hachour, O., and Bouzouia, B. (2015). Mobile manipulator path planning based on artificial potential field: Application on robuter/ulm. In *2015 4th International Conference on Electrical Engineering (ICEE)*, pages 1–6. IEEE.

IFR (2017). Executive summary world robotics 2017 industrial robots: How robots conquer industry worldwide. Frankfurt. International Federation of Robotics Press.

ISO (1998). Iso9283: Manipulating industrial robots-performance criteria and related test methods.

Kennedy, R. K. (2017). *Understanding, Measuring, and Improving Overall Equipment Effectiveness: How to Use OEE to Drive Significant Process Improvement*. Productivity Press, New York, 1st edition.

Khatib, O. (1986). Real-time obstacle avoidance for manipulators and mobile robots. *The international journal of robotics research*, 5(1):90–98.

Koppula, H. S. and Saxena, A. (2016). Anticipating human activities using object affordances for reactive robotic response. *IEEE transactions on pattern analysis and machine intelligence*, 38(1):14–29.

Mac, T. T., Copot, C., Hernandez, A., and De Keyser, R. (2016). Improved potential field method for unknown obstacle avoidance using uav in indoor environment. In *2016 IEEE 14th International Symposium on Applied Machine Intelligence and Informatics (SAMI)*, pages 345–350. IEEE.

Mittal, R. and Nagrath, I. (2003). *Robotics and control*. Tata McGraw-Hill.

Moellmann, A. H., Albuquerque, A. S., Contador, J. L., and Marins, F. A. S. (2006). Aplicação da teoria das restrições e do indicador de eficiência global do equipamento para melhoria de produtividade em uma linha de fabricação. *Revista gestão industrial*, 2(1).

Mora, M. C. and Tornero, J. (2008). Path planning and trajectory generation using multi-rate predictive artificial potential fields. In *Intelligent Robots and Systems, 2008 IEEE/RSJ International Conference on*, pages 2990–2995. IEEE.

Nawrocka, A., Nawrocki, M., and Kot, A. (2014). Fuzzy logic controller for rehabilitation robot manipulator. In *Control Conference (ICCC), 2014 15th International Carpathian*, pages 379–382. IEEE.

Pinto, L., Davidson, J., and Gupta, A. (2016). Supervision via competition: Robot adversaries for learning tasks. *arXiv preprint arXiv:1610.01685*.

Simoes, M. G. and Shaw, I. S. (2007). *Controle e Modelagem Fuzzy*. Edgard Blucher, Sao Paulo, 2nd edition.

Spong, M. W. (2006). *Robot modeling and control*, volume 3. Wiley New York.

Volpe, R. and Khosla, P. (1990). Manipulator control with superquadric artificial potential functions: Theory and experiments. *IEEE Transactions on Systems, Man, and Cybernetics*, 20(6):1423–1436.

Wang, X., Jin, Y., and Ding, Z. (2015). A path planning algorithm of raster maps based on artificial potential field. In *Chinese Automation Congress (CAC), 2015*, pages 627–632. IEEE.

Yu, K., Ohnishi, K., Kawana, H., and Usuda, S. (2015a). Modulated potential field using 5 dof implant assist robot for position and angle adjustment. In *Industrial Electronics Society, IECON 2015-41st Annual Conference of the IEEE*, pages 002166–002171. IEEE.

Yu, K., Uozumi, S., Ohnishi, K., Usuda, S., Kawana, H., and Nakagawa, T. (2015b). Stereo vision based robot navigation system using modulated potential field for implant surgery. In *Industrial Technology (ICIT), 2015 IEEE International Conference on*, pages 493–498. IEEE.